MULTISPECTRAL BACKSCATTERING : A FRACTAL-STRUCTURE PROBE

ROBERT BOTET[†] AND PASCAL RANNOU[‡]

[†] *Laboratoire de Physique des Solides - CNRS, Bâtiment 510, Université Paris-Sud Centre d'Orsay, F-91405 Orsay, France*
Tel : (33/0) 1-69 15 69 25, Fax : (33/0) 1-69 15 60 86,
E-mail : botet@lps.u-psud.fr
and
[‡] *Service d'Aéronomie, Tour 15, Boîte 102, Université Paris 6, 4 Place Jussieu, 75252 Paris Cedex 05, France*
Tel : (33/0) 1-44 27 49 70, Fax : (33/0) 1-44 27 37 76,
E-mail : pra@ccr.jussieu.fr,

We present numerical results for backscattering of electromagnetic waves by fractal aggregates of fractal dimension ≤ 2. Single-scattering analytical result shows that Fourier transform of the density-density mass correlation function of the scatterer is the main contribution of the backscattering cross-section wavelength variation, when wavelength is in the fractal range of the scattering object. This allows to conjecture that multispectral backscattering analysis could be used to measure the geometrical fractal dimension of the scatterer. Illustrative results are given by using several recently proposed numerical scattering codes accounting for multiple scattering. Applications to lidar experiments in the visible range are briefly discussed.

1 Fractal Aggregates

Aerosol particles commonly consist of disordered clusters of nanometer-size grains. To give a few examples, these are soot particles from diesel engines [1], smoke obscurants [2] or haze particles in planetary atmospheres [3]. They correspond to a variety of standard two-step coalescence scenario : in a first regime, high-temperature nucleation creates compact small grains, then low-temperature aggregation forms disordered large clusters in which the grains, previously created, keep their individuality. Only the local junctions between neighbouring grains can be structurally modified by local melting, forming necks. These small local transformations will be neglected in the following, and all the grains will be considered as identical homogeneous spheres. All what will be written below for large fractal aerosol [4] clusters can be translated to disordered fractal colloidal aggregates as well, although the dispersing fluid medium is different, but the cluster structures are basically the same [5].

In dense atmosphere, two aggregation models are relevant [6] : the irreversible Brownian Cluster-Cluster Aggregation model (BrCCA) and the Reaction-limited Cluster-Cluster Aggregation model (RCCA). The first one (BrCCA) corresponds to the experimental conditions where sticking between grains is so strong that aggregation is irreversible and rapid [7] : sticking is permanent once formed. On the other hand, the latter model (RCCA) is the case where sticking is so weak that only

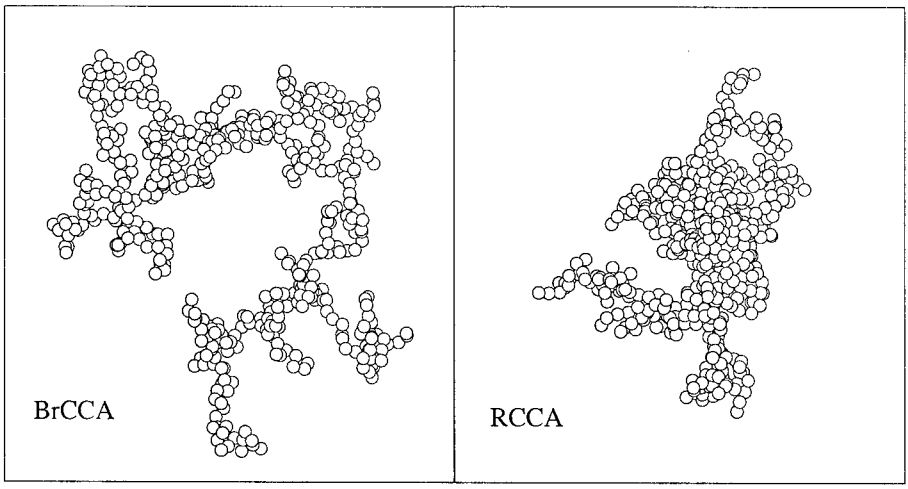

Figure 1. Fractal clusters of 512 identical particles generated respectively with the Brownian CCA model ($D_f = 1.75$), and with the Reaction-limited CCA model ($D_f = 2$)

the strongest structures are permanently formed [8] . In this slow aggregation, the clusters are more compact than for the BrCCA case. Both models lead to fractal structures, and the fractal dimensions are, respectively, $D_f = 1.75$ (for BrCCA) and $D_f = 2$ (for RCCA). Fig. 1 gives typical pictures of 3-dimensional clusters numerically built with such models.

Optical response of such structures carries informations about the fractal correlations. The most widely known is the so-called q^{-D_f}-law [9] valid for small-angle neutron- or X-scattering. This gives direct access to the fractal dimension of the clusters [10]. This law is derived in the case where scattering is so weak that multiple scattering can be neglected. It should be corrected when multiple scattering is expected to play some role - as when the refractive index is significantly different from 1, and fractal dimension larger than 2 -. Note that the value $D_f = 2$ is the expected threshold, some logarithmic corrections may arise in this case.

Properties of the scattering pattern of electromagnetic wave by such aggregate are the direct consequence of interferences between waves with different phases due to the spatial distribution of the grains. This distribution can be characterized by the distance-distribution function representing the density-density correlation function in the case of aggregates of N identical spheres [11] :

$$P(\vec{r}) = \left\langle \frac{1}{N(N-1)} \sum_{i \neq j} \delta(\vec{r} - \vec{r}_{ij}) \right\rangle \quad ,$$

where the summation runs over all pairs of distinct grains. The δ is the Dirac-distribution, and average is here over a large set of independent clusters of the same fractal dimension and the same number N of grains. This function $P(\vec{r})$, after orientation averaging, becomes a function of the variable r only. It can be

written [12] as :

$$P(r) = \frac{1}{A_{D_f} R_g^3} \left(\frac{r}{R_g}\right)^{D_f - 3} f_c\left(\frac{r}{R_g}\right) \quad , \tag{1}$$

with a positive cut-off function f_c. R_g is the radius of gyration, given by

$$R_g^2 = \frac{1}{2}\int_0^\infty r^2 P(r) 4\pi r^2 dr \quad .$$

The coefficient A_{D_f} in Eq.(1) insures proper normalization of the distance-distribution function. For simple applications, the cut-off function f_c is approximated by an exponentially decreasing function, such that [9] :

$$P(r) = \frac{1}{A_{D_f} R_g^{D_f}} r^{D_f - 3} \exp[-\frac{r}{R_g}\sqrt{\frac{D_f(D_f+1)}{2}}] \quad . \tag{2}$$

This approximation is not valid in general and a much more precise form is : $f_c(z) \sim \exp(-z_f^D/2)$ as it has been shown in [12]. The latter is useful for numerical computation, but analytic calculations can often be handled only for the exponential cut-off.

2 Electromagnetic Scattering Codes

First exact results for scattering of electromagnetic field on some large objects (*i.e.*, of size comparable to the wavelength) were obtained in the classical Mie's work [13] for spherical, homogeneous scatterers irradiated by monochromatic plane wave. The solution is then given as a series of vector spherical functions which (usually) converges. There are several natural ways to extend this result to more complicated cases. One of them is to consider a rigid assembly of such identical balls, and to wonder if one can express the scattered field knowing the exact response of any of these balls. This is the T-matrix formalism which is briefly reviewed in the following section. Another way is to consider a non-homogeneous ball, where the refractive index depends continuously on the distance to the center, for example according to the averaged density of the cluster. This method is not well known and is discussed in more details below in Sec.D.

2.1 Orientation-Averaged T-Matrix Code

In principle, for the case of rigid aggregate of homogeneous spheres, the cluster T-matrix method is the exact solution of Maxwell equations with appropriate boundary conditions [14]. Its basis is just the linearity of Maxwell equations and boundary conditions. Writing the scattered electric field in terms of usual expansion :

$$\vec{E}_{sca}(j) = \sum_{n=1}^{\infty}\sum_{m=-n}^{n} iE_{mn}[a_{mn}^j \vec{N}_{mn}^{(3)}(j) + b_{mn}^j \vec{M}_{mn}^{(3)}(j)] \quad , \tag{3}$$

with the standard notations for the spherical harmonics functions [15], the method consists then in developing all these fields over a unique ensemble of vector spherical functions, by systematic use of the addition theorem which expresses spherical

harmonic functions referring to the center of some grain into series of vector spherical functions with the origin on a reference point. All the fields, included the incident one, being expressed over the same basis of vectors, one can write self-consistently that the local field on particle j is the sum of the incident field plus all fields scattered by other particles, and obtain a set of coupled linear equations in all the expansion coefficients (a^j_{mn}, b^j_{mn}). Truncating the order of these equations at a reasonable level of accuracy, the problem reduces to an inversion of a large matrix equation. Moreover, a very efficient computational method has recently been proposed, where orientation averaging is performed analytically [17]. Since fractal clusters are essentially non-spherical, *except in a statistical meaning*, this scheme provides considerable help in the practical computation of the average scattering coefficients.

2.2 Mean-Field Mie-Code

The T-matrix equations can be substantially simplified in a mean-field approach where all the grains are supposed to scatter the *same* electromagnetic field. This has been done previously for the dipolar scattered fields [18], but this was recently extended to the Mie scattering [19], that is, with scattered fields of the form (3). In this case we have not to consider self-consistent equations between N scattered fields, but just one self-consistent equation with one (mean-field) scattered field. Inversion of a small matrix equation is needed and usually can be performed quickly on any small computer. It is difficult to judge the correctness of the mean-field hypothesis, but numerically it leads to one of the best, now available approximations for self-similar aggregates of identical grains [16]. Qualitatively, great inhomogeneities of the local fields should be avoided and this means that the system is far from any optical resonance [20]. Moreover, the geometrical structure itself should be as homogeneous as possible. This means for fractal aggregates that we have to deal only with strictly self-similar objects, like the clusters generated by the models discussed here (BrCCA and RCCA).

2.3 Discrete-Dipole Approximation

This method, known as DDA numerical method [21] , consists in dividing the scatterer into identical pieces small enough to be individually considered as electromagnetic dipoles, but large enough in order that the number of such sub-units be not too large. All these dipoles interact, and since the field radiated by each dipole is analytically simple, the method is exact, as far as space discretisation is fine enough to insure the dipolar representation be correct. Below, we used this method with one dipole per grain. This is correct if the wavelength is much larger than the radius of one grain, but as soon as the size parameter becomes of order unity, we should take several dipoles per grain, but the computations become rapidly important from both CPU time and memory points of view.

2.4 Fractally-Coated Code

This section is about a new approximate computation of the scattered properties for fractal clusters. Instead of taking the exact solution by the T-matrix method, then averaging over all possible orientations, one can decide first to average the geometric structure, yielding radially decreasing density of matter, and then to compute the scattering properties as if it was for a ball of same spherical density. More precisely, consider fractal distributions of matter with fractal dimension D_f. Suppose that these are fractal aggregates of balls of radius a. If they are statistically radially symmetric, one can identify the center of the ball closest to the center of gravity as the center of coordinates and write the average density as :

$$\begin{aligned} \rho(r) &= 1 \qquad\qquad \text{if} \qquad r \leq a \\ \rho(r) &= \left(\frac{r}{a}\right)^{D_f-3} \quad \text{if} \qquad a < r < R \\ \rho(r) &= 0 \qquad\qquad \text{if} \qquad r > R \quad , \end{aligned} \tag{4}$$

where R is a typical radius of the aggregate. The constraint on the total mass of the aggregate gives explicitly the value of R since we must have

$$M(\infty) = \int_0^R \left(\frac{r}{a}\right)^{D_f-3} 4\pi r^2 dr \quad ,$$

equal to the mass of the aggregate, namely, $M = 4\pi a^3 N/3$. This means that

$$R/a = (D_f N/3)^{1/D_f} \quad .$$

With these results in hands one can compute the electromagnetic field scattered by a ball of radial refractive index $n_{av}(r)$ given by the Maxwell-Garnett rule [15]

$$n_{av}^2(r) = \frac{n^2(1+2\rho(r)) + 2(1-\rho(r))}{n^2(1-\rho(r)) + 2 + \rho(r)} \quad ,$$

with n the refractive index for the grain. This comes from the multilayered sphere recursive equations [22] which are both stable and accurate.

2.5 Numerical Comparison Between Codes

All four methods have been implemented into numerical codes for fractal aggregates. Firstly we compare all of them, the T-matrix method being considered as giving the exact results. We present in this article a small part of this task, more systematic comparisons are in preparation [23]. We have decided to show here some comparisons for several representative values of refractive index, namely, $n = 1.5$ (non absorbing), $n = 1.5 + i * 10^{-4}$, $n = 1.5 + i * 10^{-2}$ and $n = 1.5 + i$ (strongly absorbing). Just one size is discussed, $N = 512$ - for which the fractal features are known to be well developed -, and the grain-size parameter $x = ka = 2\pi a/\lambda$ is between 10^{-4} and 1. For these parameters, the T-matrix as well as the DDA methods cannot go to values of x much larger than 1. The extinction and backscattering cross-sections are shown for the four computations in Figs. 2, and 3.

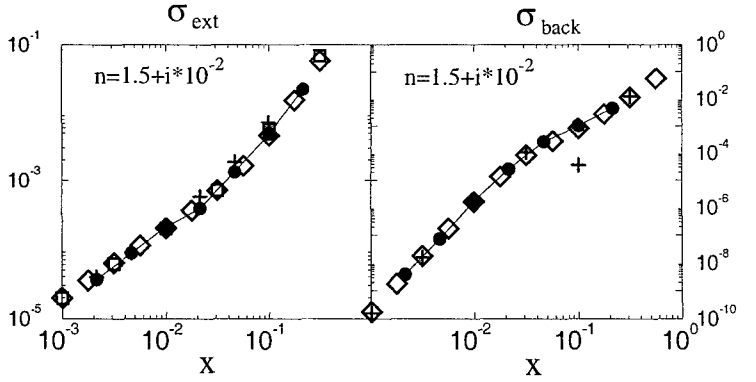

Figure 2. Numerical comparisons between the four methods described in the text, for $N = 512$ RCCA clusters of fractal dimension $D_f = 2$. The refractive index is $n = 1.5 + i * 10^{-2}$, and the grain-size parameter x varies between 10^{-3} and 1. Double-logarithmic scale, the cross-sections have all been divided by $N\pi a^2$ for normalisation. Symbols are : full circles (and line) are for T-matrix, diamonds for Mean-Field Mie, crosses for DDA, squares for fractally-coated methods, respectively.

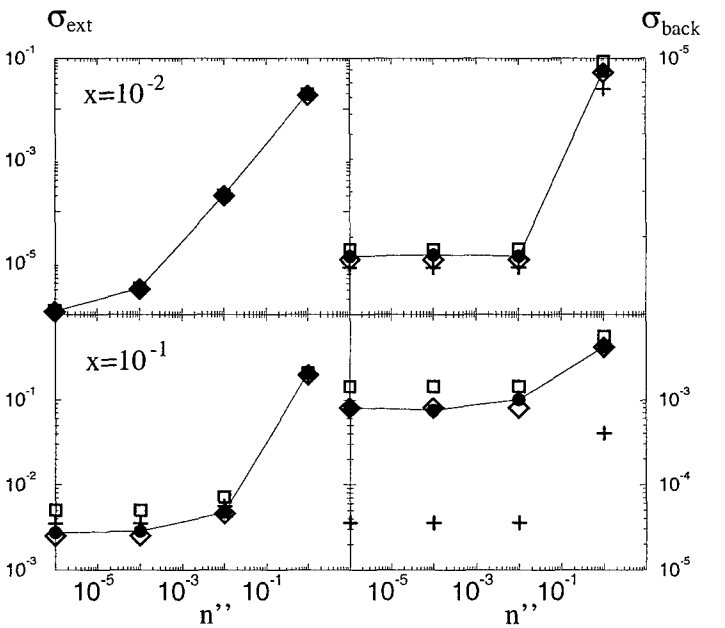

Figure 3. Numerical comparisons between the four methods described in the text, for $N = 512$ RCCA clusters of fractal dimension $D_f = 2$. The refractive index is $n = 1.5 + i * n"$, with different values of $n"$ between 0 and 1. Note that the data for $n" = 0$ (*i.e.* for the non-absorbing index : $n = 1.5$) has been shifted to $n" = 10^{-6}$ to show them on the same figure. Double-logarithmic scale, the cross-sections have all been divided by $N\pi a^2$ for normalisation. Symbols are : full circles (and line) are for T-matrix, diamonds for Mean-Field Mie, crosses for DDA, squares for fractally-coated computations respectively.

The results are quantitatively comparable even if the fractally-coated results are indeed less precise, leading to slight overestimation of the cross-sections when x becomes large. The DDA code may give wrong under-estimate values of the backscattering cross-sections, due to lack of numerical stability, as shown in the $x = 10^{-1}$ case. These results reinforce the conclusions that the Mean-Field Mie method is the most reliable approximation up to the largest values of x attainable by T-matrix code with our computers.

3 Backscattering Coefficient

The backscattering coefficient needs particular comment. This coefficient is important in some applications like lidar experiments, basically because in such experiments, one light beam is emitted and the backscattered light is analysed [24]. This kind of experiments can be handled with far scattering sources because of this simple geometry, and gives access to precise informations about remote aerosol scatterers [25]. Furthermore, backscattering is also phenomenologically known to be important to distinguish between various forms of scatterers [26].

3.1 Single-Scattering Theory

If we suppose single-scattering to be the dominant feature, and the cut-off function to be exponential, then the orientation-averaged intensity I_s of the light scattered at angle θ by fractal aggregate of size N and fractal dimension D_f, is just [9]

$$I_{sca}(N) = N I_{sca}(1) \left[1 + (N-1) \frac{\sin[(D_f - 1)\tan^{-1}(q\xi)]}{(D_f - 1)q\xi} \frac{1}{(1+q^2\xi^2)^{(D_f-1)/2}} \right] \quad (5)$$

with the modulus of the scattering vector, $q = 2k\sin(\theta/2)$, and $\xi = R_g\sqrt{2/D_f(D_f+1)}$. This formula allows to recover properly the Guinier-regime for $qa \ll 1$ and the fractal q^{-D_f}-law for $1/\xi \ll q \ll 1/a$. Moreover, for extinction, we are interested in $q = 0$ since we look at the $\theta = 0$ case, and so

$$\sigma_{ext}(N) = N\sigma_{ext}(1) \quad ,$$

as a consequence of forward coherence. More precise forms of extinction cross-section can be found in [18].

The case is totally different for backscattering since in this case, $q = 2k$, and the waves scattered by the grains do not have the same phase. More precisely :

$$\sigma_{back}(N) = N\sigma_{back}(1) \left[1 + (N-1) \frac{\sin[(D_f - 1)\tan^{-1}(2k\xi)]}{(D_f - 1)2k\xi} \frac{1}{(1+4k^2\xi^2)^{(D_f-1)/2}} \right] \quad ,$$

as an immediate consequence of (5). In particular, in the case of clusters large compared to the wavelength ($k\xi \gg 1$), the preceding formula approximates as

$$\sigma_{back}(N) \simeq N\sigma_{back}(1) \left[1 + \frac{B_{D_f}}{(ka)^{D_f}} \right] \quad ,$$

with finite numerical coefficient B_{D_f} depending only on the fractal dimension of the scatterer. This means that when ka is small enough, the ratio $\sigma_{back}(N)/N\sigma_{back}(1)$

is essentially proportional to $(ka)^{-D_f}$, or equivalently

$$\ln\left(\frac{\sigma_{back}(N)}{N\sigma_{back}(1)}\right) \sim D_f \ln(\lambda) \quad \text{for} \quad a < \lambda < R_g. \tag{6}$$

When $\lambda \ll a$, then the ratio $\sigma_{back}(N)/N\sigma_{back}(1)$ is close to 1 and its logarithm vanishes. For $\lambda \gg R_g$, the phase difference between the grains can be neglected and we recover the same coherence peak as for forward scattering [27] $\sigma_{back}(N)/N\sigma_{back}(1) \simeq N$ independently of the wavelength. Relation (6) provides a possible measure of the fractal dimension D_f of the scatterers analysed at different wavelengths. This is in principle a natural way to examine a fractal aggregate since the basic property of such an object is self-similarity. We just claim that analysing a fractal with different wavelengths correspond to investigating its structure with different length scales, and the result (6) is an illustration of this fact. A particular case of this idea has previously been proposed [28] with application to fractal Sierpinski gaskets .

3.2 Multiple-Scattering Results

So, in principle, relation (6) should give access to the fractal dimension of the clusters if one can measure the backscattering cross-section at different wavelengths in between the typical size of the grains and the typical radius of the aggregates. The result is in principle strictly valid only for the single-scattering approximation. One can wonder then if it holds also when multiple-scattering is no more negligible. In fact, we can qualitatively argue that for fractal dimensions $D_f \leq 2$, multiple scattering is expected to be small compared to single scattering. So, in this case, the signature of the fractal structure should be seen anyway, even if a bit modified. This should be checked on numerical simulations taking the multiple scattering into account.

But first, we have to be careful about the fact that the wavelength dependence of the refractive index of grain material is not generally cancelled by such simple procedure as taking the ratio $\sigma_{back}(N)/N\sigma_{back}(1)$, when multiple scattering is present. Focusing on the signature of fractal structure, we suppose here that correction is done in such a way that the refractive index of the grains can be considered as constant over the range of wavelengths. Usually, this can be done when the wavelength dependence of the refractive index of the material and the typical size of the grains are known.

Since we have shown before that the Mean-Field Mie code gives results very close to the exact T-matrix computation inside the range of analysis, we shall discuss the results of this method (Mean-Field Mie code) which can easily be used for very large values of the grain-size parameter.

Fig. 4 gives the numerical results for $N = 512$, and the two kinds of fractal aggregates : BrCCA with $D_f = 1.75$ and RCCA with $D_f = 2$, for the refractive index $n = 1.5 + i * 10^{-2}$. The single-scattering result (6) is well recovered over about one decade in both cases. This range is the expected one since for these models and $N = 512$, the values of ξ/a are about 20 and 14 for BrCCA and RCCA respectively. The left-hand plateau for the long wavelengths is the Rayleigh coherent regime

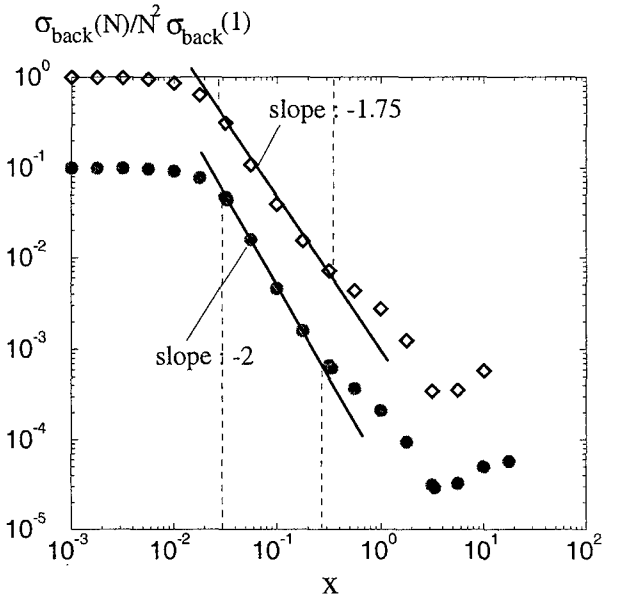

Figure 4. Sketch of the ratio $\sigma_{back}(N)/N^2\sigma_{back}(1)$ *vs* the grain-size parameter x for BrCCA (diamonds, fractal dimension = 1.75) and RCCA (circles, fractal dimension = 2), calculated with the Mean-Field Mie method. Double-logarithmic plot. The RCCA data have been divided by a factor 10 for visual separation of the two cases. The D_f-slope - derived in the single-scattering theory -, is well recovered between the dashed lines.

and in this case we expect : $\sigma_{back}(N) \simeq N^2\sigma_{back}(1)$. On the other side, for the small wavelengths, one begins to see oscillating behaviour on the curves, before the possible limiting value $\sim 1/N$. These results show clearly that the single-scattering result (6) is very robust in these cases and dominates the leading behaviour even if multiple scattering is taken into account.

4 Conclusions

We briefly reviewed in this work four theoretical methods allowing to compute either exactly or with fine accuracy the optical cross-sections of fractal aggregates. We used the corresponding numerical codes to compare their results for two sets of typical fractal clusters of fractal dimension $D_f = 1.75$ and $D_f = 2$, relevant in aerosol and colloid physics. For reasonable values of the refractive index of the material, the Mean-Field Mie method is seen to give the most accurate and reliable results, as compared to the exact T-matrix method, which is limited by the large amount of computations when the grain-size parameter becomes large.

As an application, we have studied the wavelength dependence of the backscattering cross-section for wavelengths between the size of the grains and the radius of the aggregates. It has been shown that such analysis gives access to a very particular signature of the fractal structure, and could in principle be used to estimate the

fractal dimension of the scatterers by lidar experiments, since lidar signal depends essentially of the backscattering and the extinction cross-sections of the scattering aerosols. This should give a new alternative to measure experimentally the fractal dimension of fractal aggregates by electromagnetic radiation scattering.

Note : The numerical scattering codes for fractal aggregates are available upon request from *pra@ccr.jussieu.fr* for the Mean-Field Mie and DDA methods, and from *botet@lps.u-psud.fr* for the T-matrix and fractally-coated methods. The basic T-matrix code may be found at *http://www.giss.nasa.gov/ crmim/*, and original DDA code comes from *http://www.astro.princeton.edu/ draine/scattering.html.*

References

1. Sorensen C., Cai J., Lu N., Appl. Opt. **31** (1992) p 9547-6557.
   Mengüç M., Manckavasagam S., Appl. Opt. **36** (1997) p 1337-1351.
2. Dziedzinl F., Botet R., J. Phys. II **1** (1991) p 343-352.
3. West R.A., Smith P.H., Icarus, **90** (1991) p 330-333.
   Rannou P., Cabane M., Chassefière E., Botet R., McKay C.P., Icarus, **111** (1995) p 355-372.
4. Forrest S., Witten T., J. Phys. A, **12** (1979) p L109-L117.
5. Weitz D., Lin M., Sandroff C., Surf. Sci. **158** (1985) p 147-164.
6. Jullien R., Botet R., *Aggregation and Fractal Aggregates*, World Scientific, Singapore 1987.
7. Meakin P., Phys. Rev. Lett., **51** (1983) p 1119-1122.
   Kolb M., Botet R., Jullien R., Phys. Rev. Lett., **51** (1983) p 1123-1126.
8. Kolb M., Jullien R., J. Physique Lett. **45** (1984) p L977-981.
   Brown W.D., Ball R., J. Phys. A **18** (1985) p L517-L521.
9. Teixeira J., in *On Growth and Form*, Proceedings of the NATO Advanced Study Institute, Martinus Nijhoff, Dordrecht Netherthelands 1986 p 145-162.
10. Schaefer D.W., Martin J.E., Wiltzius P., Cannell D.S., Phys. Rev. Lett., **52** (1984) p 2371-2374.
11. Meakin P., J. Phys. A **18** (1985) p L661-L666.
12. Botet R., Rannou P., Cabane M., J. Phys. A **28** (1995) p 297-316.
13. Mie G., Ann. Phys. **25** (1908) p 377-452.
14. Mackowski D.W., Proc. R. Soc. London Ser.A **433** (1991) p 599-614.
    Xu Y.-L., Appl. Opt. **34** (1995) p 4573-4588.
15. Bohren C.F., Huffman D.R., *Absorption and Scattering of Light by Small Particles*, John Wiley & Sons, New-York 1983.
16. Rannou P., Cabane M., Botet R., Chassefière E., J. Geophys. Research, **102** (1997) p 10997-11013.
17. Khlebtsov N.G., Appl. Opt., **31** (1992) p 5359-5365.
    Mackowski D.W., Mishchenko M.I., J. Opt. Soc. Am. **13** (1996) p 2266-2278.

18. Berry M.V., Percival I.C., Optica Acta **33** (1986) p 577-591.
19. Botet R., Rannou P., Cabane M., Appl. Opt. **36** (1997) p 8791-8797.
20. Shalaev V.M., Botet R., Tsai D.P., Kovacs J., Moskovits M., Physica A **207** (1994) p 197-207.
21. Purcell E.M., Pennypacker, Astrophys. J. **186** (1973) p 705-514.
Draine B.T., Flatau P.J., J. Opt. Soc. Am A **11** (1994) p 1491-1499.
22. Kerker M., *The Scattering of Light and Other Electromagnetic Radiations*, Acad. San Diego, California 1969.
Wu Z.S., Wang Y.P., Radio Science **26** (1991) p 1393-1401.
23. Botet R., Rannou P., in preparation.
24. Klett J.D., Appl. Opt., **20** (1981) p 211-220.
Kasparian J., Frejafon E., Rambaldi P., Yu J., Vezin B., Wolf J.-P., Atm. Env. **32** (1998) p 2957-2967.
25. Frejafon E., Kasparian J., Rambaldi P., Vezin B., Yu J., Wolf J.-P., Appl.Opt. **37** (1998) p 2231-2237.
26. Barber P.W., Massoudi H., Aerosol Sci. Technol. **1** (1982) p 303-310.
27. Asakura T., Ishii K., Iwai T., Uozumi J., Appl. Opt. **37** (1998) p 5014-5018.
28. Lakhtakia, Messier R., Varadan V.V., Varadan V.K., J. Phys. A **20** (1987) p 1617-1619.